

Constitutive Analysis of Dynamic Recrystallization and Flow Behavior of a Medium Carbon Nb-V Microalloyed Steel

Wen-fei Shen, Li-wen Zhang, Chi Zhang, Yi-feng Xu, and Xin-hua Shi

(Submitted September 4, 2015; in revised form February 29, 2016; published online March 31, 2016)

The dynamic recrystallization (DRX) and flow behavior of a medium carbon Nb-V microalloyed steel was investigated using hot isothermal compression experiments in a wide range of temperatures (1123–1473 K) and strain rates ($0.01\text{--}10\text{ s}^{-1}$). The flow stress curves were analyzed comprehensively, and it was found that the flow stress of this steel is higher than C-Mn steel and V microalloyed steel. All the curves obtained can be ranged into three principal types: work hardening, dynamic recovery, and DRX. The DRX behavior of this steel was investigated, including critical strain, kinetics of DRX, and microstructure. The constitutive equation to predict the flow stress of the tested steel was also developed, and the analysis result indicates that the developed model has a high accuracy in predicting the flow stress during hot deformation.

Keywords constitutive equation, dynamic recrystallization, flow stress, hot deformation, medium carbon Nb-V microalloyed steel

1. Introduction

The medium carbon Nb-V microalloyed steel, as a typical non-quenched and tempered steel, has been widely used for cutting shaft parts in machine tool and other machinery industry (Ref 1, 2). This steel can be directly used for cutting products after shaped into parts, as the mechanical properties are obtained at the end of the forming process. So an important saving of costs and energy can be reached by reducing the number of operations (such as heat treatment, and straightening.) (Ref 3–6). Recently, more and more attention has been paid on this kind of steel.

This steel is produced by thermo-mechanical controlled processing consisting of controlled rolling and controlled cooling. The rolling temperature is from about 850 to 1200 °C. Several interconnect metallurgical phenomena such as WH, DRV, and DRX inevitably occur during hot deformation process (Ref 7). The hot deformation process directly affects the microstructure evolution of the material and the mechanical properties of the formed product. So, in order to improve the properties of this steel, parameters of the hot forming process must be controlled carefully and the hot deformation behavior of this steel must be investigated clearly (Ref 8, 9).

In the past, some researches about microalloyed steel have already been done. Xie et al. (Ref 10), Bao et al. (Ref 11), Cho

et al. (Ref 12), etc., have studied the DRX, static recrystallization (SRX), and metadynamic recrystallization (MDRX) behavior of Nb microalloyed steel. Wei et al. (Ref 13) and Zhao et al. (Ref 14) investigated the DRX behavior of V microalloyed steel. Lan et al. (Ref 15) studied the DRX and SRX behavior of Nb-Ti microalloyed steel. There are also some studies about the flow behavior of V microalloyed steel (Ref 4, 16–20). However, for hot deformation behavior of the medium carbon Nb-V microalloyed steel, few studies have been reported, especially for systematic researches about both DRX behavior and flow behavior of the steel.

In this paper, the isothermal hot compression tests of a medium carbon Nb-V microalloyed steel in a wide range of strain rates and deformation temperatures were conducted. Based on the experiment data, the DRX behavior of this steel was investigated. The constitutive equation to predict the flow stress of the tested steel was also developed and flow stress predicted by the developed constitutive equation was compared with the experimental ones.

2. Experimental Procedures

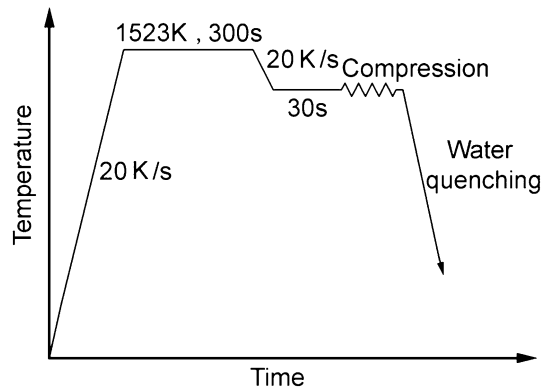
The chemical composition of the tested steel in this paper is given in Table 1. In order to perform the isothermal hot compression tests, cylindrical specimens with a diameter of 8 mm and a height of 12 mm were machined. To reduce the friction between the anvils and the end faces of the specimens during the compression process, tantalum foils with thickness of 0.05 mm were placed between anvils and specimens.

Isothermal hot compression tests were conducted on a Gleeble-1500 thermo-mechanical simulator. Figure 1 shows the schematic of the isothermal hot deformation process. Before compression, the specimens were heated to 1523 K at the rate of 20 K/s and held for 300 s to make the alloyed elements completely dissolve and ensure uniform temperature, during this process the initial ferrite and pearlite phases transformed to single austenite phase. Then, the specimens were cooled to the testing temperatures (from 1123 to 1473 K with an interval of

Wen-fei Shen, Li-wen Zhang, and Chi Zhang, School of Materials Science and Engineering, Dalian University of Technology, No.2, Ling Gong Road, Dalian 116023, China; and Yi-feng Xu and Xin-hua Shi, Suxin Special Steel Group Co., Ltd., No.28, Gang Cheng Road, Tong an Town, High-Tech Industrial Development Zone, Suzhou 215151, China. Contact e-mail: commat@mail.dlut.edu.cn.

Table 1 Chemical composition of the tested steel (wt.%)

| C | Si | Mn | P | S | Cr | V | Nb | N |
|-----------|------|------|--------|--------|------|------|------|--------|
| 0.38-0.45 | 0.45 | 1.50 | ≤ 0.02 | ≤ 0.04 | 0.25 | 0.05 | 0.02 | 0.0083 |

**Fig. 1** Schematic of the isothermal hot deformation process

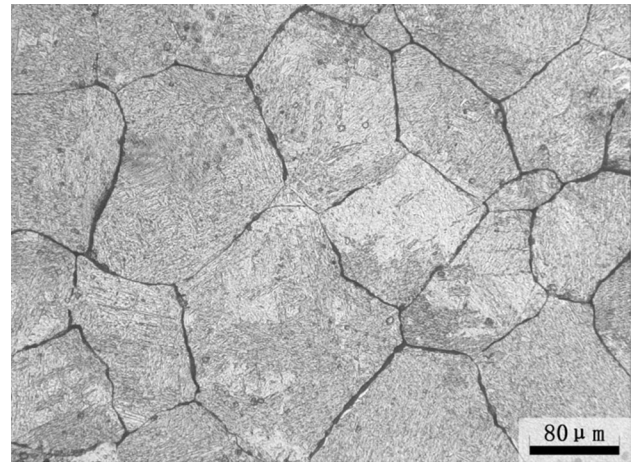
50 K) at the rate of 20 K/s and held for 30 s to eliminate the temperature gradient. Subsequently, the specimens were compressed to a strain of 0.8 at the testing temperatures with the constant strain rates (0.01, 0.1, 1, and 10 s⁻¹). After compression, the specimens were water quenched immediately to room temperature. The initial austenite grain size of the steel after austenite homogenization is shown in Fig. 2.

3. Results and Discussion

3.1 Analysis of Flow Stress Curves

A series of typical true strain-stress curves obtained from the hot compression tests are shown in Fig. 3. It can be seen that the flow stress was greatly influenced by the deformation temperature and strain rate. The flow stress increases with the increase of strain rate and the decrease of temperature. This is because that lower strain rates and higher temperatures provide longer time for energy accumulation and higher mobility at boundaries for the nucleation and growth of dynamically recrystallized grains and dislocation annihilation (Ref 21). Meanwhile, all the curves obtained can be ranged into three types depending on the relationship between stress and strain, as shown in Fig. 4: WH, characterized by increasing stress with strain (like curve 1123 K, 1 s⁻¹); DRV, characterized by saturation stress with increasing strain (like curve 1223 K, 0.1 s⁻¹); and DRX, characterized by an observed peak stress (like curve 1473 K, 0.01 s⁻¹) (Ref 22). Besides, compared to the C-Mn steel (Ref 17) and V microalloyed steel (Ref 4, 18, 19), the flow stress of this medium carbon Nb-V microalloyed steel is about 10-40 MPa higher than them. This may be due to the high solute strengthening and precipitation strengthening effect of microalloyed element Nb (Ref 23).

As shown in Fig. 4, the typical true strain-stress curves of DRX of the tested steel can be divided into two stages by critical strain ε_c . In stage I, the true stress increases rapidly with the increasing strain at initial deformation process and then the increasing rate decreases. This is because that the

**Fig. 2** The initial austenite grain size of the steel after austenite homogenization

WH caused by the dislocation generation and multiplication is greater than the DRV caused by the dislocation climbing, sliding, and cross-slip. In stage II, the true stress is influenced by the interaction of WH, DRV, and DRX. At the beginning of this stage, the true stress increases to a peak stress with a decreased increasing rate. Because in this region, the WH is dominant until the balance of hardening and softening, including DRV and DRX, is reached. Then, the true stress gradually decreases to a steady value. The reason is that in this region the hardening is weaker than softening until a new balance of them is reached.

3.2 Constitutive Analysis of DRX Behavior

3.2.1 Zener-Hollomon Parameter and Hot Working Equation. Hot deformation of metals is a thermally activated process, and the flow stress is mainly affected by deformation temperature, strain rate, and strain. Recently, the Arrhenius equation is widely used to analysis the relationship between deformation temperature, strain rate, and flow stress, particularly at high temperature (Ref 24):

$$\dot{\varepsilon} = AF(\sigma) \exp(-Q/RT), \quad (\text{Eq 1})$$

where

$$F(\sigma) = \begin{cases} \sigma^{n_1} & \alpha\sigma < 0.8 \\ \exp(\beta\sigma) & \alpha\sigma > 1.2, \\ [\sinh(\alpha\sigma)]^n & \text{for all } \sigma \end{cases}$$

in which, $\dot{\varepsilon}$ is the strain rate, Q is the activation energy of hot deformation, R is the universal gas constant, T is the absolute temperature, σ is the flow stress, and A , α , β , n_1 , and n are material constants, $\alpha = \beta/n_1$.

The effects of the temperatures and strain rate on the deformation behaviors can be represented by Zener-Hollomon parameter (Z) in an exponential equation (Ref 25). Z parameter is written as follows:

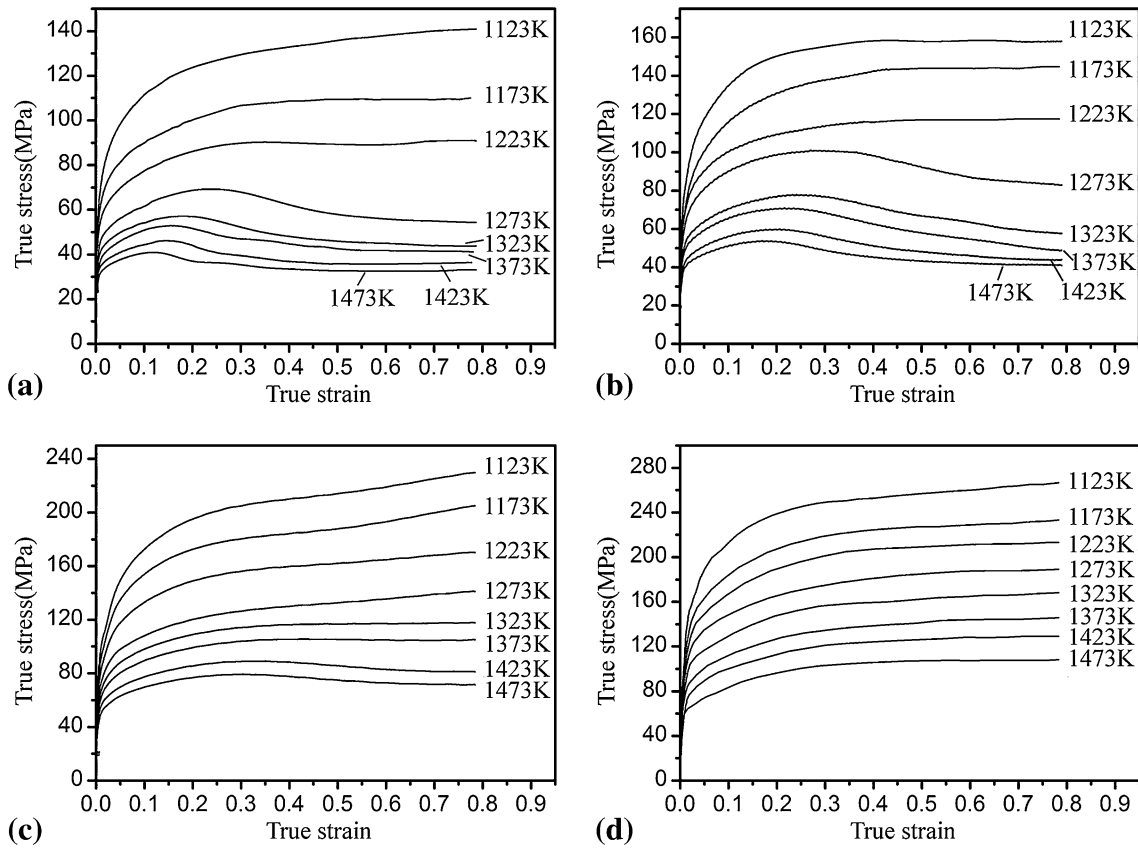


Fig. 3 Flow stress curves of the tested steel obtained under different strain rates (a) 0.01 s⁻¹ (b) 0.1 s⁻¹ (c) 1 s⁻¹ and (d) 10 s⁻¹

$$Z = \dot{\epsilon} \exp(Q/RT). \quad (\text{Eq } 2)$$

In order to determine the parameters in the equations, the peak stress is employed to the linear regression process. Equation 1 can be expressed as power law equation and exponential law equation at low and high stress levels, respectively. Then the following equations can be obtained,

$$\dot{\epsilon} = A_1 \sigma_p^{n_1}, \quad (\text{Eq } 3)$$

$$\dot{\epsilon} = A_2 \exp(\beta \sigma_p), \quad (\text{Eq } 4)$$

where A_1 and A_2 are material constant. Taking the logarithm of both sides of Eq 3 and 4, respectively, then Eq 5 and 6 can be gained,

$$\ln \dot{\epsilon} = n_1 \ln \sigma_p + \ln A_1, \quad (\text{Eq } 5)$$

$$\ln \dot{\epsilon} = \beta \sigma_p + \ln A_2. \quad (\text{Eq } 6)$$

Substituting the value σ_p and $\dot{\epsilon}$ into the Eq 5 and 6. Then the relationships between strain rate and stress can be obtained in Fig. 5. The value of β and n_1 can be obtained from the mean slopes of $\ln \dot{\epsilon} - \sigma_p$ and $\ln \dot{\epsilon} - \ln \sigma_p$, respectively. The value of β is 0.0915 MPa⁻¹ and n_1 is 6.8195. So, the value of α is derived, $\alpha = \beta/n_1 = 0.01342 \text{ MPa}^{-1}$.

The hyperbolic sine law of $F(\sigma)$ has been verified that it can accurately describe hot deformation behavior at both low stress and high stress level (Ref 26, 27). Therefore, the following equations can be derived,

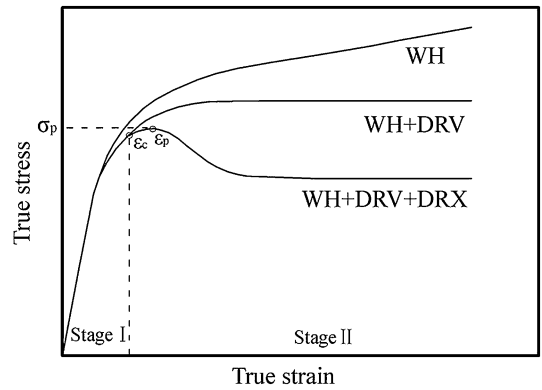


Fig. 4 Three types of the flow stress curves

$$\dot{\epsilon} = A \sinh(\alpha \sigma_p)^n \exp(-Q/RT). \quad (\text{Eq } 7)$$

By taking the logarithm of both sides of Eq 7 give

$$\ln \dot{\epsilon} = \ln A + n \ln [\sinh(\alpha \sigma_p)] - Q/RT. \quad (\text{Eq } 8)$$

Then the following equations can be derived,

$$\frac{1}{n} = \left[\frac{\partial \ln [\sinh(\alpha \sigma_p)]}{\partial \ln \dot{\epsilon}} \right], \quad (\text{Eq } 9)$$

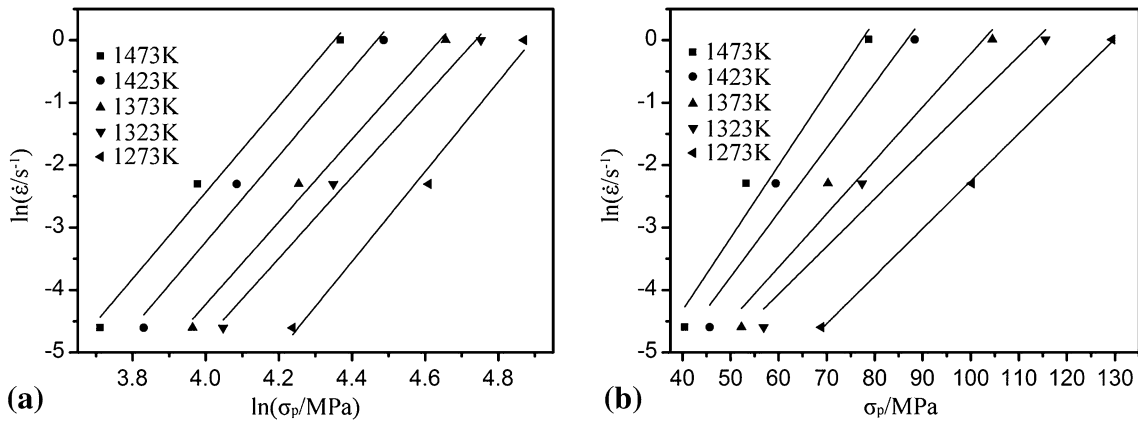


Fig. 5 The relationships of (a) $\ln \dot{\epsilon} - \ln \sigma_p$ and (b) $\ln \dot{\epsilon} - \sigma_p$

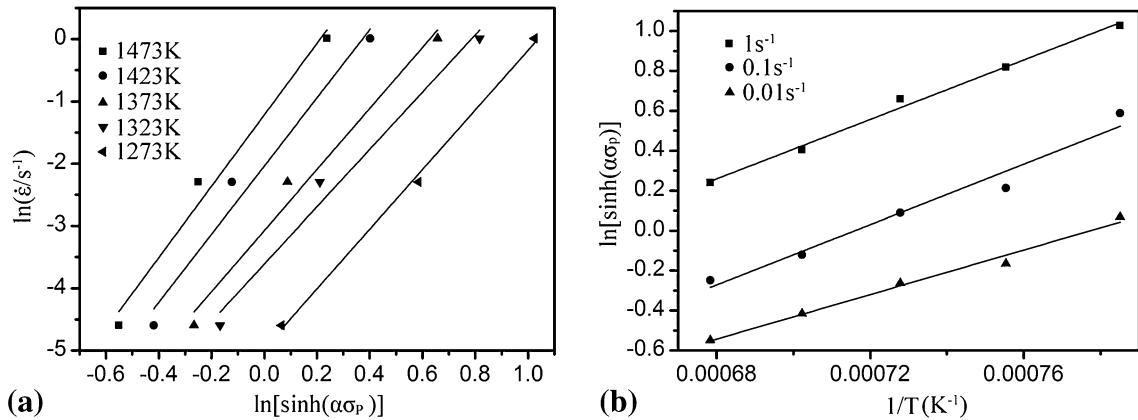


Fig. 6 The relationships of (a) $\ln \dot{\epsilon} - \ln[\sinh(\alpha\sigma_p)]$ and (b) $\ln[\sinh(\alpha\sigma_p)] - 1/T$

$$Q = Rn \left[\frac{\partial \ln[\sinh(\alpha\sigma_p)]}{\partial (1/T)} \right] \quad (\text{Eq 10})$$

The relationships of $\ln \dot{\epsilon} - \ln[\sinh(\alpha\sigma_p)]$ and $\ln[\sinh(\alpha\sigma_p)] - 1/T$ are shown in Fig. 6(a) and (b), respectively. It is easy to obtain the value of n and Q from the slopes of the plots as 5.10 and 318.31 kJ/mol, respectively. Activation energy Q is an important material constant which can reflect the deformation difficulty degree in hot deformation. Medina and Hernandez (Ref 28) have investigated that the value of Q of 0.36C-Mn steel and C-Mn-0.043 V steel are 271 and 275 kJ/mol, respectively. And they are lower than the value of tested steel in this paper. This indicates that vanadium addition has no obvious effect on the activation energy, and the microalloyed element Nb can increase the activation energy dramatically. The reason may be that activation energy varied with atomic volumes of the microalloyed elements, which occupy substitutional sites ($V_V < V_{Nb}$). And the atomic radius of V is slightly greater than that of Fe, therefore, the influence of V is much lower than that of Nb.

According to the obtained parameters, the material constant A in Eq 1 is calculated as 6.9×10^{10} . Then the hot working equation can be expressed as

$$\dot{\epsilon} = 6.9 \times 10^{10} \sinh(0.0134\sigma_p)^{5.10} \exp(-318310/RT). \quad (\text{Eq 11})$$

3.2.2 Critical Strain, Kinetics Model, and Microstructure of DRX. The critical strain of material is the prerequisite for the research of DRX. According to the previous researches (Ref 4, 14), the relationship between ϵ_c and Z is showed as below

$$\epsilon_c = A_3 Z^k, \quad (\text{Eq 12})$$

then substituting the values of ϵ_c obtained from the flow stress curves and Z into the Eq 12, and the relationship between critical strain and Z parameter can be obtained as shown in Fig. 7. It can be seen that the $\ln \epsilon_c$ and $\ln Z$ relation is linear and the slope and intercept of the regressed curve are 0.164 and 0.002997, respectively. So the relationship between ϵ_c and Z can be expressed as below

$$\epsilon_c = 2.997 \times 10^{-3} Z^{0.164}. \quad (\text{Eq 13})$$

In this research, the modified Avrami equation (Ref 29-31) which incorporates an empirical time constant for 50% recrystallization $t_{0.5}$ is used to describe the DRX volume fraction X of the tested steel. The DRX volume fraction X is expressed as

$$X = 1 - \exp\left[-0.693(t/t_{0.5})^{k_d}\right], \quad (\text{Eq 14})$$

$$t_{0.5} = A_4 \dot{\varepsilon}^{A_5} \exp(\bar{Q}/RT), \quad (\text{Eq 15})$$

where t is the deformation time after the critical strain, and k_d , A_4 , A_5 , and \bar{Q} are constants.

As seen from Fig. 3, DRX is an important softening mechanism. But it is difficult to determine the DRX volume fraction X by microstructural observations directly. In this research, the DRX volume fraction X is derived from the flow curves, which is defined as the following (Ref 32-35).

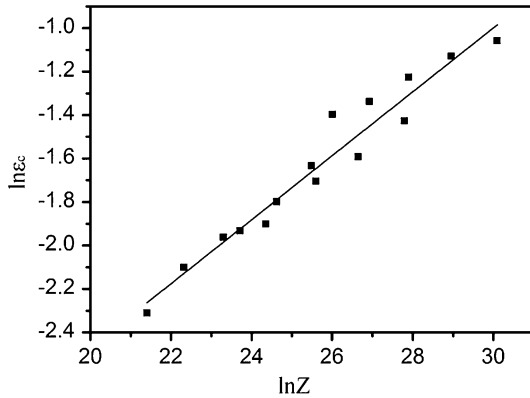


Fig. 7 The relationship between $\ln \varepsilon_c$ and $\ln Z$

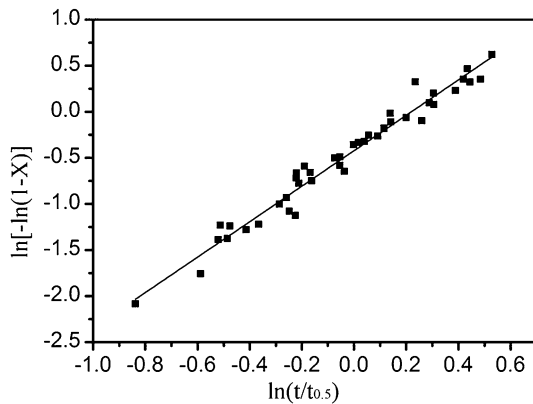
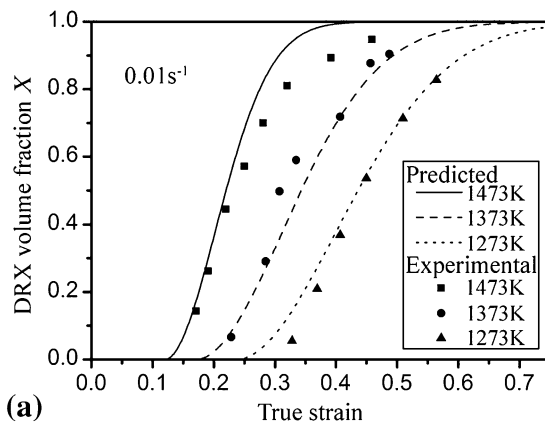


Fig. 8 Relationship between $\ln[-\ln(1-X)]$ and $\ln(t/t_{0.5})$



$$X = \frac{\sigma_p - \sigma}{\sigma_p - \sigma_s}, \quad (\text{Eq 16})$$

where σ_p is the peak stress and σ_s is the steady state stress. The $\sigma_p - \sigma_s$ term represents the maximum achievable softening fraction, and the $\sigma_p - \sigma$ represents the flow softening from peak to the stress of σ . Note that the effect of DRV on flow softening is not considered and the initiation of DRX is considered occurred from σ_p . This assumption simplifies the Avrami analysis with acceptable level of accuracy (Ref 36, 37).

Equations 14 and 15 can be written as Eq 17 and 18, respectively.

$$\ln[-\ln(1-X)] = \ln 0.693 + k_d \ln(t/t_{0.5}), \quad (\text{Eq 17})$$

$$\ln t_{0.5} = \ln A_4 + A_5 \ln \dot{\varepsilon} + \bar{Q}/RT. \quad (\text{Eq 18})$$

The relationship between $\ln[-\ln(1-X)]$ and $\ln(t/t_{0.5})$ is shown in Fig. 8. The value of k_d can be determined by the linear slope of the curve as 2.012. Then, the values of A_4 , A_5 and \bar{Q} can be obtained from the linear regression according to Eq 18. And the mean value of A_4 , A_5 , and \bar{Q} are 0.0257, -0.857 and 29315.62, respectively. So the kinetic model of DRX for the tested steel can be established as follows,

$$X = 1 - \exp\left[-0.693(t/t_{0.5})^{2.012}\right], \quad (\text{Eq 19})$$

$$t_{0.5} = 0.0257 \dot{\varepsilon}^{-0.857} \exp(29315.62/RT). \quad (\text{Eq 20})$$

Based on the derived DRX kinetic model, the effect of deformation temperature, strain rate, and strain on the DRX volume fraction X is shown in Fig. 9. It can be seen that with the true strain increasing X increases slowly at first and then the increasing rate gradually increased, and reduced in the end. Moreover, the increasing rate of X increases with increasing temperature and decreasing strain rate. Comparisons between predicted and experiment results are also presented. The predicted results agree with experimental ones, which indicate that the developed model can give a accurate results of DRX of the tested steel.

Some researchers have verified that the DRX grain size is influenced by Z parameter. The DRX grain size increases with the decreasing Z , i.e., the DRX grain size increases with the increasing deformation temperature and decreasing strain rate.

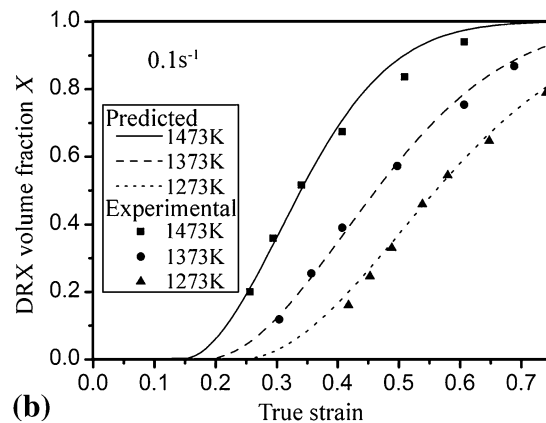


Fig. 9 Experimental and predicted DRX volume fraction X with strain rate of (a) 0.01 s^{-1} and (b) 0.1 s^{-1}

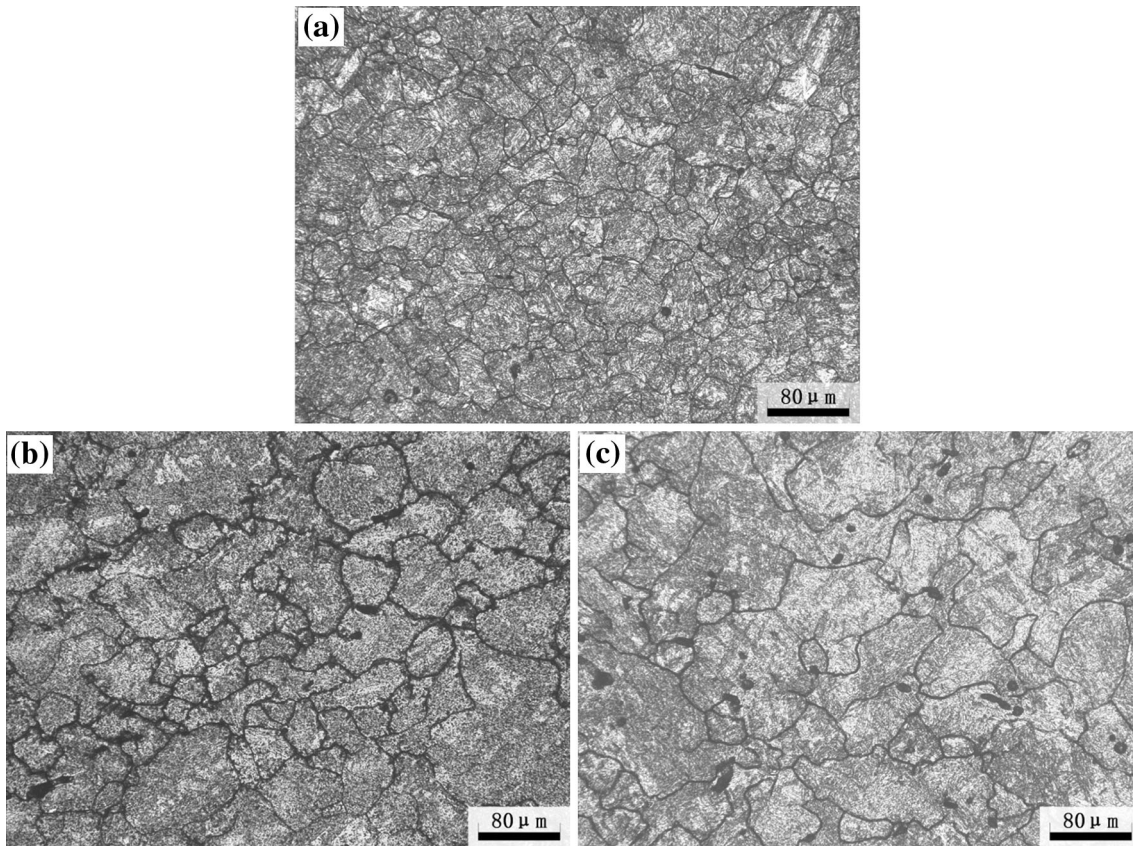


Fig. 10 The recrystallized austenite grain size after hot isothermal compression at the temperature of 1373 K and strain rates of (a) 1 s^{-1} (b) 0.1 s^{-1} and (c) 0.01 s^{-1}

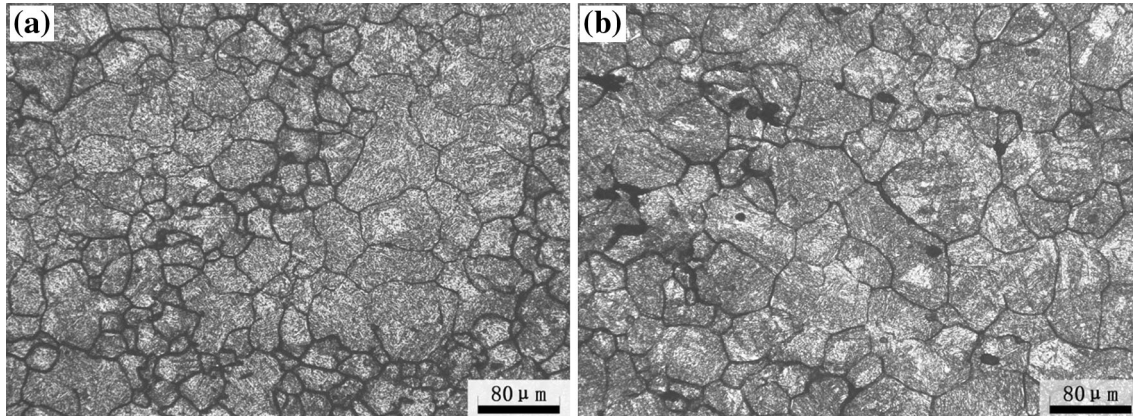


Fig. 11 The recrystallized austenite grain size after hot isothermal compression at the strain rate of 1 s^{-1} and temperatures of (a) 1423 K and (b) 1473 K

Figure 10 and 11 show the recrystallized austenite grain size after hot isothermal compression at different conditions. It can be seen that the DRX grain size increases from strain rate of 1 – 0.01 s^{-1} with the same temperature of 1373 K, and the DRX grain size increases obviously with the increasing of temperature with the same strain rate of 1 s^{-1} . In order to model the dependence of the grain size on Z parameter, the following equation is used,

$$D_s = BZ^{-k} \quad (\text{Eq 21})$$

Although regression analysis, as shown in Fig. 12, the value of B and k can be obtained as 12751.222 and 0.211. So the DRX grain size model can be expressed as below,

$$D_s = 12751.222Z^{-0.211} \quad (\text{Eq 22})$$

3.3 Constitutive Analysis of Flow Stress Behavior

The flow stress in steel during hot temperature has two softening mechanisms: dynamic recovery (DRV) and dynamic recrystallization (DRX). When the strain fails to reach the critical strain, DRV is the only softening mechanism. When the strain exceeds the critical strain, DRX occurs (Ref 22, 38).

When no DRX occurring, the dislocation density supposed to be the coupled effects of generation by WH and annihilation by DRV. The dependence of the dislocation density on strain can be written as follows:

$$\frac{d\rho}{d\varepsilon} = U - \Omega\rho, \quad (\text{Eq 23})$$

where ρ is the dislocation density, and U and Ω are the parameters related to the strain that represent the work hardening and softening terms, respectively.

The relationship between flow stress and dislocation density can be described as follows (Ref 39):

$$\sigma = \alpha\mu b\sqrt{\rho}, \quad (\text{Eq 24})$$

where α , μ , and b are constants with the value of 0.7, 8.1×10^4 , and 2.6×10^{-10} , respectively.

Utilizing Eq (23) and (24), the constitutive equation for flow stress during DRV process can be obtained:

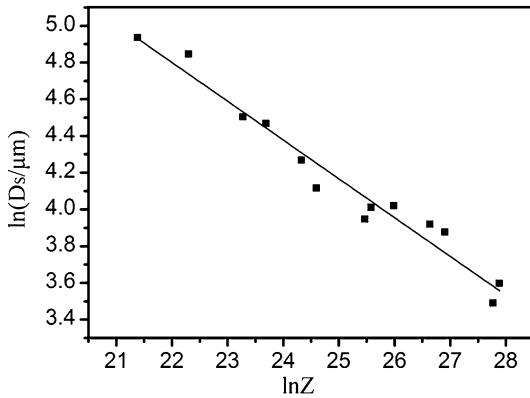


Fig. 12 The relationship between $\ln D_s$ and $\ln Z$

$$\sigma_r = [(\alpha\mu b)^2 \rho_0 e^{-\Omega\varepsilon} + (\alpha\mu b)^2 (U/\Omega)(1 - e^{-\Omega\varepsilon})]^{0.5}, \quad (\text{Eq 25})$$

where σ_r is the flow stress during DRV process, ρ_0 is the initial dislocation density, $1.0 \times 10^{-12} \text{ m}^{-2}$.

The parameters Ω and $(\alpha\mu b)^2 U$ are dependent on the deformation temperature and strain rate, the following typical equation are used to describe the relationships:

$$\Omega = A_\Omega \dot{\varepsilon}^{m_\Omega} \exp(-Q_\Omega/RT), \quad (\text{Eq 26})$$

$$(\alpha\mu b)^2 U = A_U \dot{\varepsilon}^{m_U} \exp(Q_U/RT). \quad (\text{Eq 27})$$

In order to regress the constants in Eq 26 and 27, several groups of stress and strain values were obtained from the flow stress curves. Although multiple linear regression, the values of A_Ω , m_Ω , and Q_Ω are 280, -0.1 , and 35966.4 J/mol . The values of m_U and Q_U/R are the slopes of the plots in the $\ln[(\alpha\mu b)^2 U]$ versus $\ln \dot{\varepsilon}$ and $\ln[(\alpha\mu b)^2 U]$ versus $1/T$, as shown in Fig. 13(a) and (b). Then the values of A_U , m_U , and Q_U can be obtained as 344.5 , 0.19 , and 63269.5 J/mol .

When DRX occurring, dislocation density decreases with the DRX fraction increasing. The flow stress can be described as following:

$$\sigma_d = \sqrt{\sigma_r^2 - X(\sigma_r^2 - \sigma_{ss}^2)}, \quad (\text{Eq 28})$$

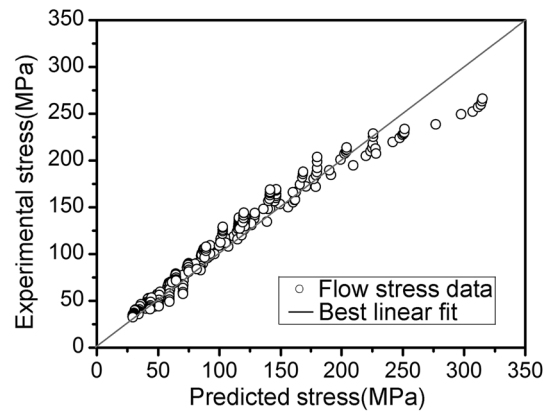


Fig. 14 Correlation between the experimental and predicted flow stress data

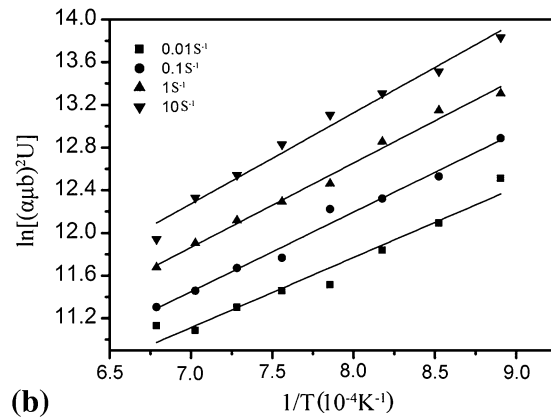
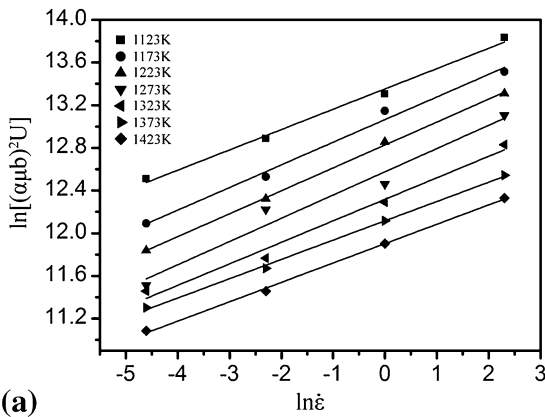


Fig. 13 The relationship between $\ln[(\alpha\mu b)^2 U]$ and $\ln \dot{\varepsilon}$ (a); $\ln[(\alpha\mu b)^2 U]$ and $1/T$ (b)

where σ_d is the flow stress during the DRX period. σ_{ss} is the steady state stress after DRX. The steady state stress can be defined as following:

$$\sigma_{ss} = A_{ss} [\dot{\epsilon} \exp(Q_{ss}/RT)]^{m_{ss}}, \quad (\text{Eq 29})$$

where A_{ss} , m_{ss} , and Q_{ss} are constants, and they can be regressed by the experimental data. The values of A_{ss} , m_{ss} , and Q_{ss} are 0.938, 0.172, and 301.4 kJ/mol, respectively.

Then, the constitutive equation for DRV can be obtained as follows:

$$\sigma_r = [217.3 \exp(-\Omega\epsilon) + 1.23 \times \dot{\epsilon}^{0.29} \exp(11937/T)(1 - \exp(-\Omega\epsilon))]^{0.5}. \quad (\text{Eq 30})$$

The constitutive equation for DRX can be obtained as follows:

$$\sigma_d = \begin{cases} \sigma_r \epsilon \leq \epsilon_c \\ \sqrt{\sigma_r^2 - X(\sigma_r^2 - 0.88 \times \dot{\epsilon}^{0.344} \exp(301440/RT))^{0.344}} \epsilon > \epsilon_c \end{cases} \quad (\text{Eq 31})$$

In order to evaluate the accuracy of the developed constitutive equation in predicting the flow stress during hot deformation, standard statistical parameters of correlation coefficient (R) is used to quantify the predictability of the constitutive equation. It can be expressed as:

$$R = \frac{\sum_{i=1}^N (E_i - \bar{E})(P_i - \bar{P})}{\sqrt{\sum_{i=1}^N (E_i - \bar{E})^2 \sum_{i=1}^N (P_i - \bar{P})^2}}, \quad (\text{Eq 32})$$

where E_i is the experimental data and P_i is the predicted value obtained from the constitutive equation. \bar{E} and \bar{P} are the mean values of E and P , respectively. N is the total number of data employed in the investigation. As is shown in Fig. 14, a good correlation ($R = 0.973$) is obtained, which indicates that the developed constitutive equation is appropriate to predict the flow stress of the steel during hot deformation.

4. Conclusions

Isothermal hot compression experiments of a medium carbon Nb-V microalloyed steel were performed in a wide range of temperatures (1123–1473 K) and strain rates (0.01 – 10 s^{-1}). DRX behavior and constitutive equation of flow stress of the tested steel was carried out. The following conclusions can be obtained:

- (1) Deformation temperature and strain rate have great influence on flow stress of the steel. The flow stress increases with the increase of strain rate and the decrease of temperature. All the flow curves obtained can be ranged into three principal types: WH, characterized by increasing stress with strain; DRV, characterized by saturation stress with increasing strain; and DRX, characterized by an observed peak stress.
- (2) The hot working equation of the tested steel was obtained as $\dot{\epsilon} = 6.9 \times 10^{10} \sinh(0.0134\sigma_p)^{5.10} \exp(-318310/RT)$. Activation energy Q is calculated as 318.310 kJ/mol

which is higher than C-Mn steel and V microalloyed steel due to the addition of microalloyed element Nb.

- (3) The DRX behavior of the tested steel was investigated. The relationship of critical strain on Z was obtained as $\epsilon_c = 2.997 \times 10^{-3} Z^{0.164}$. The kinetics model was developed as $X = 1 - \exp[-0.693(t/t_{0.5})^{2.012}]$, $t_{0.5} = 0.02566 \dot{\epsilon}^{-0.857} \exp(29315.62/RT)$, and the predicted DRX volume fraction X agree with experimental ones. The relationship of DRX grain size D_s on Z was obtained as $D_s = 12751.222 Z^{-0.211}$.
- (4) Constitutive equation for flow stress of the tested steel was established. The correlation coefficient R of the experimental and predicted flow stress is 0.973 which indicates that the developed constitutive equation can accurately predict the flow stress of tested steel.

Acknowledgment

The authors are very grateful to the financial support received from the Suzhou Suxin Special Steel Group Co., Ltd.

References

1. M. Jahazi and B. Eghbali, The Influence of Hot Forging Conditions on the Microstructure and Mechanical Properties of Two Microalloyed Steels, *J. Mater. Process. Technol.*, 2001, **113**, p 594–598
2. F. Bakkali El Hassani, A. Chenaouia, R. Dkiouak, L. Elbakkali, and A. Alomar, Characterization of Deformation Stability of Medium Carbon Microalloyed Steel During Hot Forging Using Phenomenological and Continuum Criteria, *J. Mater. Process. Technol.*, 2008, **199**, p 140–149
3. Y. Luo, J.M. Peng, H.B. Wang, and X.C. Wu, Effect of Tempering on Microstructure and Mechanical Properties of a Non-quenched Bainitic Steel, *Mater. Sci. Eng., A*, 2010, **527**(15), p 3427–3433
4. S.D. Gu, L.W. Zhang, J.H. Ruan, P.Z. Zhou, and Y. Zhen, Constitutive Modeling of Dynamic Recrystallization Behavior and Processing Map of 38MnVS6 Non-quenched Steel, *J. Mater. Eng. Perform.*, 2014, **23**(3), p 1062–1068
5. L. Ceschini, A. Marconi, C. Martini, A. Morri, and A. Di Schino, Tensile and Impact Behavior of a Microalloyed Medium Carbon Steel: Effect of the Cooling Condition and Corresponding Microstructure, *Mater. Des.*, 2013, **45**, p 171–178
6. Ahmet Kaynar, S. Gündüz, and M. Türkmen, Investigation on the Behavior of Medium Carbon and Vanadium Microalloyed Steels by Hot Forging Test, *Mater. Des.*, 2013, **51**, p 819–825
7. J.L. Liu, W.D. Zeng, Y.J. Lai, and Z.Q. Jia, Constitutive Model of Ti17 Titanium Alloy with Lamellar-Type Initial Microstructure During Hot Deformation Based on Orthogonal Analysis, *Mater. Sci. Eng., A*, 2014, **597**, p 387–394
8. Y.C. Lin, M.S. Chen, and J. Zhong, Microstructural Evolution in 42CrMo Steel During Compression at Elevated Temperatures, *Mater. Lett.*, 2008, **62**, p 2132–2135
9. S.M. Abbasi and A. Shokuhfar, Prediction of Hot Deformation Behaviour of 10Cr-10Ni-5Mo-2Cu Steel, *Mater. Lett.*, 2007, **61**, p 2523–2526
10. G.L. Xie, X.T. Wang, and L. Chen, Microstructural Modelling of Dynamic Recrystallisation in Nb Microalloyed Steels, *Mater. Sci. Technol.*, 2012, **28**, p 778–782
11. S.Q. Bao, G. Zhao, C.B. Yu, Q.M. Chang, C.L. Ye, and X.P. Mao, Recrystallization behavior of a Nb-Microalloyed Steel During Hot Compression, *Appl. Math. Model.*, 2011, **35**, p 3268–3275
12. S.H. Cho, K.B. Kang, and J.J. Jonas, The Dynamic, Static and Metadynamic Recrystallization of a Nb-microalloyed Steel, *ISIJ Int.*, 2001, **41**(1), p 63–69
13. H.L. Wei, G.Q. Liu, X. Xiao, and M.H. Zhang, Dynamic Recrystallization Behavior of a Medium Carbon Vanadium Microalloyed Steel, *Mater. Sci. Eng., A*, 2013, **573**, p 215–221

14. B.C. Zhao, T. Zhao, G.Y. Li, and Q. Lu, The Kinetics of Dynamic Recrystallization of a Low Carbon Vanadium-Nitride Microalloyed Steel, *Mater. Sci. Eng., A*, 2014, **604**, p 117–121
15. L.Y. Lan, C.L. Qiu, D.W. Zhao, X.H. Gao, and L.X. Du, Dynamic and Static Recrystallization Behavior of Low Carbon High Niobium Microalloyed Steel, *J. Iron. Steel Res. Int.*, 2011, **18**(1), p 55–60
16. J.M. Cabrera, A. AlOmar, J.M. Prado, and J.J. Jonas, Modeling the Flow Behavior of a Medium Carbon Microalloyed Steel Under Hot Working Conditions, *Metall. Mater. Trans. A*, 1997, **28**(11), p 2233–2243
17. H.L. Wei, G.Q. Liu, and M.H. Zhang, Physically Based Constitutive Analysis to Predict Flow Stress of Medium Carbon and Vanadium Microalloyed Steels, *Mater. Sci. Eng., A*, 2014, **602**, p 127–133
18. J. Wang, W.L. Ma, Z. Chu, and Q. Zhang, Constitutive Model for F45 V Microalloyed Forging Steel at High Temperature, *J. Iron. Steel Res. Int.*, 2014, **21**(4), p 464–468
19. Z. Akbari, H. Mirzadeh, and J.-M. Cabrera, A Simple Constitutive Model for Predicting Flow Stress of Medium Carbon Microalloyed Steel During Hot Deformation, *Mater. Des.*, 2015, **77**, p 126–131
20. H.Y. Li, Y.H. Li, D.D. Wei, J.J. Liu, and X.F. Wang, Constitutive Equation to Predict Elevated Temperature Flow Stress of V150 Grade Oil Casing Steel, *Mater. Sci. Eng., A*, 2011, **530**, p 367–372
21. Y.C. Lin, M.S. Chen, and J. Zhong, Prediction of 42CrMo Steel Flow Stress at High Temperature and Strain Rate, *Mech. Res. Commun.*, 2008, **35**, p 142–150
22. Y. Tao, E.L. Yu, and Y.Q. Zhao, Constitutive Modeling for Flow Stress of 55SiMnMo Bainite Steel at Hot Working Conditions, *Mater. Des.*, 2013, **50**, p 574–580
23. H.L. Wei and G.Q. Liu, Effect of Nb and C on the Hot Flow Behavior of Nb Microalloyed Steels, *Mater. Des.*, 2014, **56**, p 437–444
24. C.M. Sellars and W.J. Mcgert, On Mechanism of Hot Deformation, *Acta Metall.*, 1966, **14**(9), p 1136–1138
25. C. Zener and J.H. Hollomon, Effect of Strain Rate upon Plastic Flow of Steel, *J. Appl. Phys.*, 1944, **15**, p 22–32
26. S. Mandal, V. Rakesh, P.V. Sivaprasad, S. Venugopal, and K.V. Kasiviswanathan, Constitutive Equations to Predict High Temperature Flow Stress in a Ti-Modified Austenitic Stainless Steel, *Mater. Sci. Eng., A*, 2009, **500**, p 114–121
27. C. Phaniraj, D. Samantaray, S. Mandal, and A.K. Bhaduri, A New Relationship Between the Stress Multipliers of Garofalo Equation for Constitutive Analysis of Hot Deformation in Modified 9Cr-1Mo (P91) Steel, *Mater. Sci. Eng., A*, 2011, **528**, p 6066–6071
28. S.F. Medina and C.A. Hernandez, General Expression of the Zener-Hollomon Parameter as a Function of the Chemical Composition of Low Alloy and Microalloyed Steels, *Acta Mater.*, 1996, **44**, p 137–148
29. B.H. Lee, N.S. Reddy, J.T. Yeom, and C.S. Lee, Flow Softening Behavior During High Temperature Deformation of AZ31 Mg Alloy, *J. Mater. Process. Technol.*, 2007, **187**, p 766–769
30. G. Kugler and R. Turk, Study of the Influence of Initial Microstructure Topology on the Kinetics of Static Recrystallization Using a Cellular Automata Model, *Comput. Mater. Sci.*, 2006, **37**, p 284–291
31. J.J. Jonas, X. Quelenec, L. Jiang, and É. Martin, The Avrami Kinetics of Dynamic Recrystallization, *Acta Mater.*, 2009, **57**(9), p 2748–2756
32. M.H. Wang, Y.F. Li, W.H. Wang, J. Zhou, and A. Chiba, Quantitative Analysis of Work Hardening and Dynamic Softening Behavior of Low Carbon Alloy Steel Based on the Flow Stress, *Mater. Des.*, 2013, **45**, p 384–392
33. H. Mirzadeh and A. Najafizadeh, The Rate of Dynamic Recrystallization in 17-4 PH Stainless Steel, *Mater. Des.*, 2010, **31**, p 4577–4583
34. A. Momeni, H. Arabi, A. Rezaei, H. Badri, and S.M. Abbasi, Hot Deformation Behavior of Austenite in HSLA-100 Microalloyed Steel, *Mater. Sci. Eng., A*, 2011, **528**, p 2158–2163
35. Z.Y. Zeng, L.Q. Chen, F.X. Zhu, and X.H. Liu, Dynamic Recrystallization Behavior of a Heat-Resistant Martensitic Stainless Steel 403Nb During Hot Deformation, *J. Mater. Sci. Technol.*, 2011, **27**, p 913–919
36. M. El Wahabi, J.M. Cabrera, and J.M. Prado, Hot Working of Two AISI, 304 Steels: A Comparative Study, *Mater. Sci. Eng., A*, 2003, **343**, p 116–125
37. M. El Wahabi, L. Gavard, F. Montheillet, J.M. Cabrera, and J.M. Prado, Effect of Initial Grain Size on Dynamic Recrystallization in High Purity Austenitic Stainless Steels, *Acta Mater.*, 2005, **53**, p 4605–4612
38. S. Mandal, A.K. Bhaduri, and V.S. Sarma, A Study on Microstructural Evolution and Dynamic Recrystallization During Isothermal Deformation of a Ti-Modified Austenitic Stainless Steel, *Metall. Mater. Trans. A*, 2011, **42**, p 1062–1072
39. D.S. Svyetlichnyy, The Coupled Model of a Microstructure Evolution and a Flow Stress Based on the Dislocation Theory, *ISIJ Int.*, 2005, **45**, p 1187–1193